frontiers in Chemistry

ORIGINAL RESEARCH
published: 02 July 2018
doi: 10.3389/fchem.2018.00260

Two Novel Small Molecule Donors and the Applications in Bulk-Heterojunction Solar Cells

Xin Qi[1], Yuan-Chih Lo[2], Yifan Zhao[1], Liyang Xuan[1], Hao-Chun Ting[2], Ken-Tsung Wong[2], Mostafizur Rahaman[3], Zhijian Chen[1,4], Lixin Xiao[1,4] and Bo Qu[1,4]**

[1] State Key Laboratory for Artificial Microstructures and Mesoscopic Physics, Department of Physics, Peking University, Beijing, China, [2] Department of Chemistry, National Taiwan University, Taipei, Taiwan, [3] Department of Chemistry, King Saud University, Riyadh, Saudi Arabia, [4] New Display Device and System Integration Collaborative Innovation Center of the West Coast of the Taiwan Strait, Fuzhou, China

Two novel small molecules **DTRDTQX** and **DTIDTQX**, based on ditolylaminothienyl group as donor moiety and quinoxaline as middle acceptor moiety with different terminal acceptor groups were synthesized and characterized in this work. In order to study the photovoltaic properties of **DTRDTQX** and **DTIDTQX**, bulk-heterojunction solar cells with the configuration of FTO/c-TiO_2/**DTRDTQX**(or **DTIDTQX**):C_{70}/MoO_3/Ag were fabricated, in which **DTRDTQX** and **DTIDTQX** acted as the donors and neat C_{70} as the acceptor. When the weight ratio of **DTRDTQX**:C_{70} reached 1:2 and the active layer was annealed at 100°C, the optimal device was realized with the power conversion efficiency (PCE) of 1.44%. As to **DTIDTQX**:C_{70}-based devices, the highest PCE of 1.70% was achieved with the optimal blend ratio (**DTIDTQX**:C_{70} = 1:2) and 100°C thermal annealing treatment. All the experimental data indicated that **DTRDTQX** and **DTIDTQX** could be employed as potential donor candidates for organic solar cell applications.

Keywords: bulk-heterojunction, small molecule, donor, solar cell, ditolylaminothienyl, quinoxaline

OPEN ACCESS

Edited by:
Chuanlang Zhan, Institute of Chemistry (CAS), China

Reviewed by:
Xiaozhang Zhu, Institute of Chemistry (CAS), China
Daniel Glossman-Mitnik, Centro de Investigación en Materiales Avanzados, Mexico

***Correspondence:**
Ken-Tsung Wong
kenwong@ntu.edu.tw
Bo Qu
bqu@pku.edu.cn

Specialty section:
This article was submitted to Organic Chemistry, a section of the journal Frontiers in Chemistry

Received: *09 March 2018*
Accepted: *11 June 2018*
Published: *02 July 2018*

Citation:
Qi X, Lo Y-C, Zhao Y, Xuan L, Ting H-C, Wong K-T, Rahaman M, Chen Z, Xiao L and Qu B (2018) Two Novel Small Molecule Donors and the Applications in Bulk-Heterojunction Solar Cells. Front. Chem. 6:260. doi: 10.3389/fchem.2018.00260

INTRODUCTION

Recently, organic solar cells (OSCs) based on bulk-heterojunction structure have attracted much attention due to the distinctive characteristics of low cost, easy fabrication, flexibility and light weight, etc. (Gustafsson et al., 1992; Shaheen et al., 2001; Chen and Cao, 2009). Compared with polymers employed in solar cells, small molecule donors have the advantage of less batch-to-batch variation, well-defined molecular structure, easier purification, etc. (You et al., 2013; Chen et al., 2014, 2015; He et al., 2015; Zhou et al., 2015). Therefore, much work focused on small molecule donors and the photovoltaic performance of OSCs was improved accordingly (Sun et al., 2011; Liu et al., 2013; Love et al., 2013; Coughlin et al., 2014). In general, the active layers of the solar cells consisted of small molecule donors and fullerene/fullerene derivative acceptors (Chen et al., 2012; Huang et al., 2016). In order to optimize the photovoltaic characteristics of OSCs, narrow band-gap and deep highest occupied molecular orbital (HOMO) of small molecule donors should be considered, which resulted in broad absorption and high open-circuit voltage (V_{oc}) of devices. Then, various small molecules composed of electron rich moieties (donor, "D") and electron deficient moieties (acceptor, "A"), have been reported with the molecular configuration such as D-A (Roquet et al., 2006), A-D-A (Schulze et al., 2006), D-A-A (Lin et al., 2011) and D-A-D conjugated structures. In this regard, the HOMO and lowest unoccupied molecular orbital (LUMO) of the small molecules were effectively tuned, mainly due to the intramolecular charge transfer (ICT) between donors and acceptors (Zhang et al., 2011).

Herein, the photovoltaic properties of two novel small molecule donors (named **DTRDTQX** and **DTIDTQX**, **Figure 1**) based on D-A-A structure were studied in this work. **DTIDTQX** or **DTRDTQX** consisted of ditolylaminothienyl group as the donor moiety, quinoxaline as middle acceptor moiety with different terminal acceptor groups such as 1,3-indandione or 3-ethylrhodanine, respectively. To investigate the photovoltaic properties of the small molecules, bulk-heterojunction (BHJ) solar cells based on **DTRDTQX** or **DTIDTQX** as the donor together with C_{70} as the acceptor were fabricated and the optimal cells showed PCE of 1.44 and 1.70%, respectively.

EXPERIMENTAL

Materials and Characterization

All materials in this work were purchased commercially, except for the tailor made **DTRDTQX** and **DTIDTQX** donors. The commercial materials were used without further purification.

Scheme 1 depicts the synthesis of **DTIDTQX** and **DTRDTQX**. By following the protocols established by Krebs et al. (Jorgensen and Krebs, 2005) and Janssen et al. (Bijleveld et al., 2009), we could get 4-bromo-7-methyl-2,1,3-benzothiadiazole (**3**). Then the hetereocyclic **3** was converted to diamine intermediate **4** by treating Fe/HCl, which was then followed by condensation with glyoxal to afford 5-bromo-8-methylquinoxaline (**5**) without further purification. The 8-bromoquinoxaline-5-carbaldehyde (**7**) was synthesized by benzylic bromination with N-bromosuccinimide (NBS) initiated by azobisisobutyronitrile (AIBN) and followed by hydrolysis with $CaCO_3$ in H_2O/acetonitrile (Lin et al., 2011). Aldehyde **7** was reacted with N,N-di-p-tolyl-5-(tri-n-butylstannyl)-thiophen-2-amine (**8**) through Stille coupling reaction and gave key intermediate **9**. Finally, the condensation of **9** with 1,3-indandione and 3-ethylrhodanine via Knöevenagel reaction afforded **DTIDTQX** and **DTRDTQX**, respectively. The absorption spectra were measured with JASCO V-670 spectrophotometer. Themogravimetric analysis (TGA) was determined on a TA Instruments Model TGA Q500 V20.13 (build 39) with a heating rate of 10°C/min. Differential Scanning Calorimeter (DSC) was carried out at a heating rate of 10°C/min on a TA Instruments Model DSC Q100 V9.9 (build 303). The thickness of the films was evaluated using a surface profilometer. The electrochemical cyclic voltammetry (CV) was recorded by a CHI619B potentiostat with glassy carbon electrode, Pt wire and Ag/AgCl which were used as the working electrode, counter electrode, and reference electrode, respectively, further calibrated with the ferrocene/ferrocenium (Fc/Fc^+) redox couple. The oxidation waves were recorded in CH_2Cl_2 (for 1.0 mM) with 0.1 M tetrabutylammonium hexafluorophosphate ($^nBuNPF_6$) as supporting electrolyte, while reductive waves were recorded in THF (for 1.0 mM) with 0.1 M tetrabutylammonium perchlorate ($^nBuNClO_4$) as supporting electrolyte.

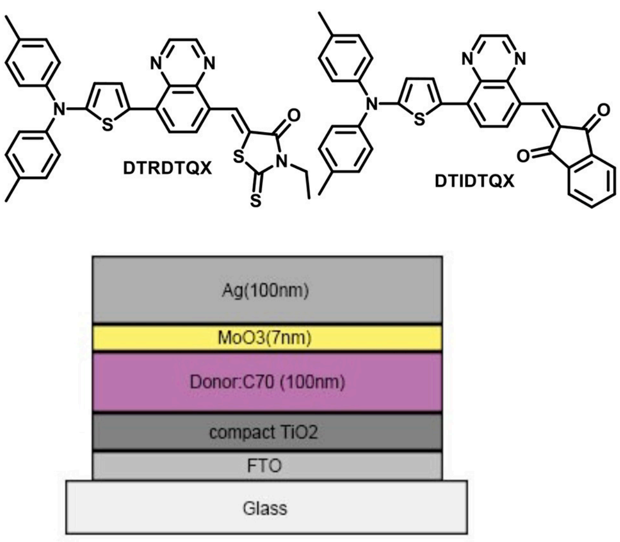

FIGURE 1 | Molecular structures of **DTRDTQX** and **DTIDTQX**, and the configuration of OSCs.

Solar Cell Fabrication and Characterization

In order to investigate the photovoltaic properties of **DTRDTQX** and **DTIDTQX**, the OSCs with the configuration of FTO/c-TiO_2/**DTRDTQX**(or **DTIDTQX**):C_{70}/MoO_3/Ag were fabricated as shown in **Figure 1**. The compact TiO_2 layer in OSCs acted as the electron transporting layer (Heo et al., 2015) and MoO_3 as the hole buffer layer. As to the photoactive layers, **DTRDTQX** and **DTIDTQX** served as the donors and C_{70} as the acceptor, respectively. The FTO cathode was pre-cleaned in an ultrasonic cleaner with deionized water, acetone and alcohol for 15 min respectively and then treated with oxygen plasma for 15 min. The TiO_2 films were fabricated according to the literatures (Kim et al., 2012; Zhang et al., 2016) and sintered at 500°C for 15 min in a muffle furnace. And then, the TiO_2 films were naturally cooled to room temperature. Blended solutions (total concentration: 20 mg/ml) of **DTRDTQX**(or **DTIDTQX**):C_{70} in *ortho*-dichlorobenzene (oDCB) were spin-coated (700 rpm, 18 s) onto FTO/TiO_2 substrates in a glove box and then thermal annealed at 100°C or 150°C. The effect of thermal annealing on the photovoltaic properties of the active layers was also studied in this work. Finally, 7 nm MoO_3 buffer layers and 100 nm Ag anodes were thermal evaporated successively below 10^{-6} Torr. The photovoltaic performance of the OSCs were evaluated by current density-bias voltage (J-V) measurement (using a Keithley 2400 source meter) under AM 1.5G simulated solar illumination (Newport model 94021A, 100 mW cm^{-2}).

RESULTS AND DISCUSSION

Thermal Property

Thermal properties of the two small molecules were investigated by TGA measurement as shown in **Figure 2** and the thermal decomposition temperatures (T_d, 5% weight loss) were evaluated to be 362°C and 312°C for DTRDTQX and DTIDTQX respectively, indicating the good thermal stability of the small molecules. According to the DSC plots shown in **Figure 3**, the melting temperatures (T_m) were evaluated to be 187.8°C and

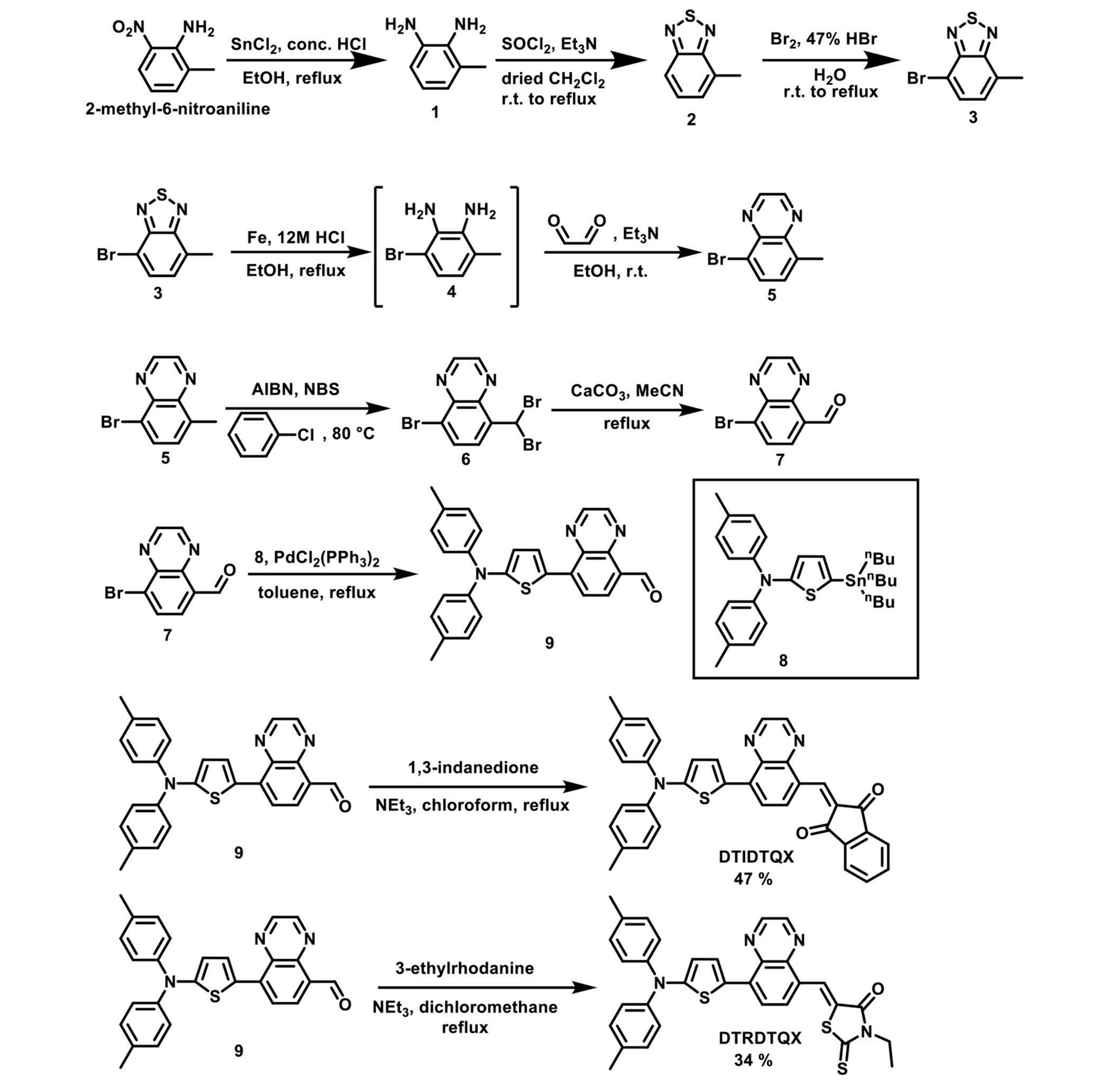

SCHEME 1 | Synthetic route of **DTIDTQX** and **DTRDTQX**.

263.3°C for DTRDTQX and DTIDTQX, respectively. Moreover, the glass transition temperatures (T_g) were measured to be 94.0°C and 149.7°C for DTRDTQX and DTIDTQX, respectively. Therefore, both DTRDTQX and DTIDTQX were stable donors for OSCs due to their decent thermal stability.

Absorption Properties

The UV-Vis absorption of **DTIDTQX** and **DTRDTQX** in CH_2Cl_2 were shown in **Figure 4** and the corresponding data were summarized in **Table 1**. The compounds showed broad band absorption from 480 to 750 nm with high extinction coefficient ($3.3–3.5 \times 10^4$ $M^{-1}cm^{-1}$) in the visible range (450–700 nm). **DTIDTQX** absorbed longer wavelength than **DTRDTQX** (631 vs. 588 nm), mainly due to the stronger electron withdrawing ability of 1,3-indanedione group than that of N-ethylrhodanine group.

Electrochemical Properties

The electrochemical properties of **DTRDTQX** and **DTIDTQX** were studied with cyclic voltammetry (CV) as shown in

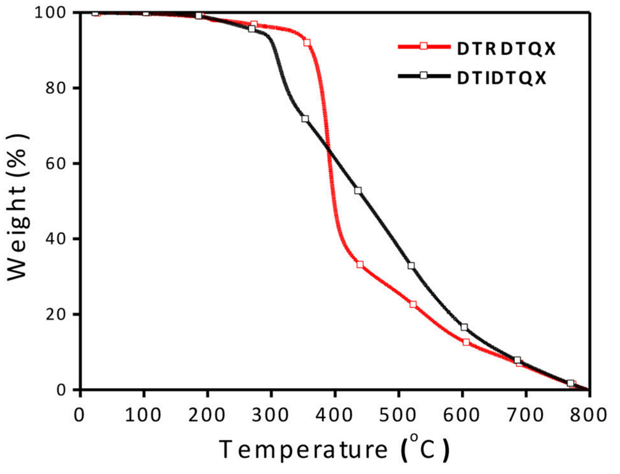

FIGURE 2 | TGA diagrams of **DTRDTQX** (up) and **DTIDTQX** (down).

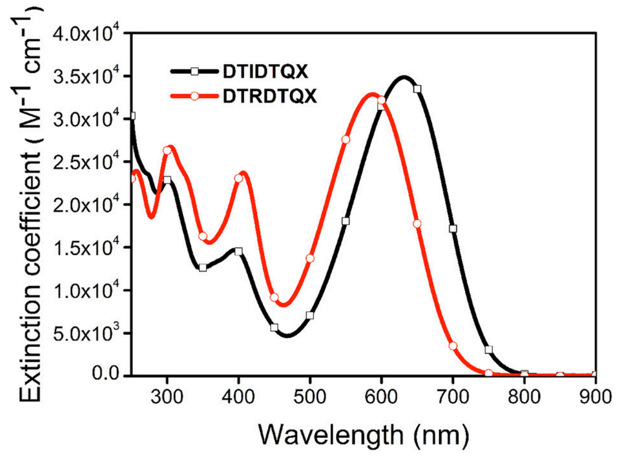

FIGURE 4 | UV-Vis absorption spectra of **DTIDTQX** and **DTRDTQX** in CH_2Cl_2.

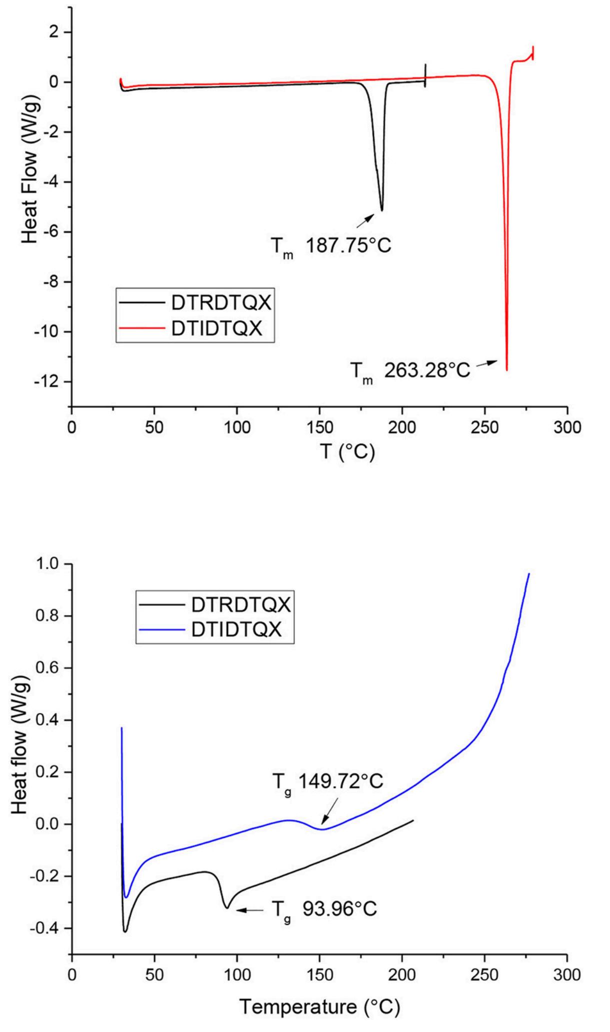

FIGURE 3 | Differential scanning calorimetry measurements of **DTRDTQX** and **DTIDTQX**.

Figure 5. In addition, the energy levels as well as the band gaps of **DTRDTQX** and **DTIDTQX** were summarized in **Table 1**. With the oxidation and reduction potentials recorded, the HOMO and LUMO levels of the two materials could be calculated (HOMO = −5.1 eV − E^{ox}_{onset}, LUMO = −5.1 eV − E^{red}_{onset}), which were −5.33 eV, −3.96 eV for **DTIDTQX** and −5.29 eV, −3.59 eV for **DTRDTQX** respectively. Interestingly, the HOMO and LUMO levels of **DTIDTQX** were both deeper than those of **DTRDTQX**. The phenomenon implied that the electron withdrawing ability of 1,3-indanedione group was stronger than that of N-ethylrhodanine group, which was consistent with the observation of UV-Vis absorption. The energy levels of the materials used in the OSCs were depicted in **Figure 6**. The large gap between the low-lying HOMO level (−5.33 eV) of **DTIDTQX** and LUMO (−4.20 eV) of C_{70} was evaluated to be 1.13 eV, which resulted in the large V_{oc} (0.71 V) of the optimal **DTIDTQX**-based OSCs in this work. Furthermore, the electrochemical energy band gap (ΔE^{CV}) of **DTIDTQX** was 0.33 eV lower than that of **DTRDTQX** and strong absorption of **DTIDTQX** active layer in red region could be realized, which was matched well with the UV-Vis absorption spectrum shown in **Figure 4**. Therefore, the light-harvesting capability as well as the photovoltaic performance of **DTIDTQX**-based devices could be superior to that of **DTRDTQX**-based counterparts, which will be discussed further in following.

Photovoltaic Properties

To study the photovoltaic properties of the small molecules, OSCs with the structure of FTO/c-TiO_2/donor:C_{70}/MoO_3/Ag were fabricated. The weight ratios of **DTRDTQX**:C_{70} and **DTIDTQX**:C_{70} varied from 1:1 to 1:3 and the corresponding J-V curves of the OSCs were shown in **Figures 7**, **8**. All the photovoltaic data of OSCs were summarized in **Table 2**. When the weight ratio of **DTRDTQX**:C_{70} reached 1:2 and the photoactive layer was thermal annealed at 100°C, the

TABLE 1 | Physical properties of **DTIDTQX** and **DTRDTQX**.

Compounds	λ_{abs} solution (nm)[a] (ε, $M^{-1}cm^{-1}$)	ΔE^{opt} sol. (eV)[a]	E^{ox}_{onset} (V)[b]	E^{red}_{onset} (V)[b]	ΔE^{CV} (eV)	HOMO (eV)[b]	LUMO (eV)[b]	Td (°C)
DTIDTQX	631 (34,900)	1.97	0.23	−1.14	1.37	−5.33	−3.96	312
DTRDTQX	588 (32,800)	2.11	0.19	−1.32	1.70	−5.29	−3.59	361

[a]*Measured in CH_2Cl_2 solution (10^{-5} M) and the value was estimated from the onset.* [b]*Estimated from the HOMO (−5.1 eV) (Cardona et al., 2011) of Fc^+/Fc as reference.* [c]*Temperature corresponding to 5% weight loss obtained from TGA analysis.*

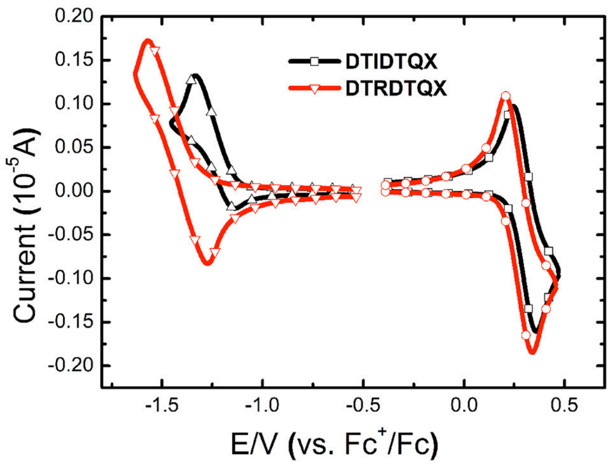

FIGURE 5 | Cyclic voltammograms of **DTIDTQX** and **DTRDTQX**.

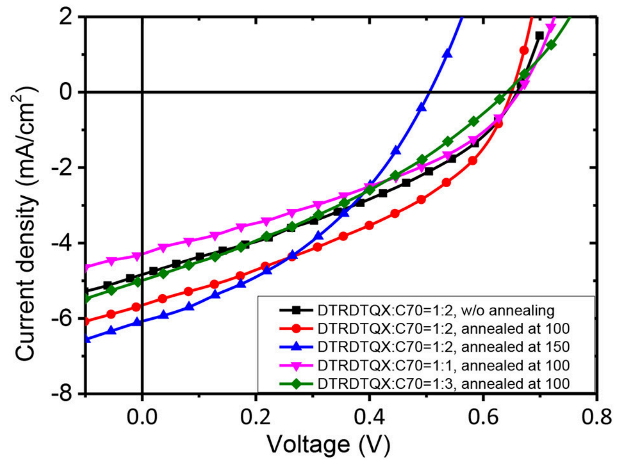

FIGURE 7 | The J-V curves of **DTRDTQX**-based devices.

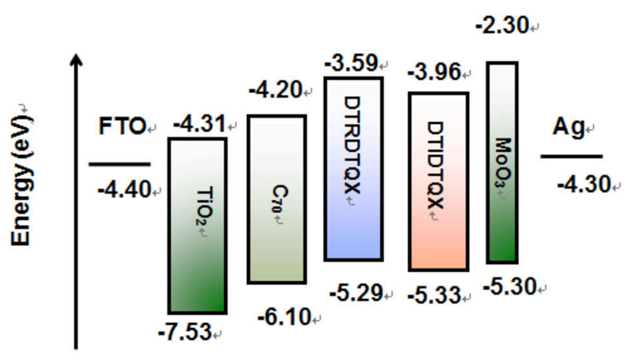

FIGURE 6 | The energy levels of the materials used in the OSCs (Lau et al., 2013; Zhang et al., 2013; Xiao et al., 2016).

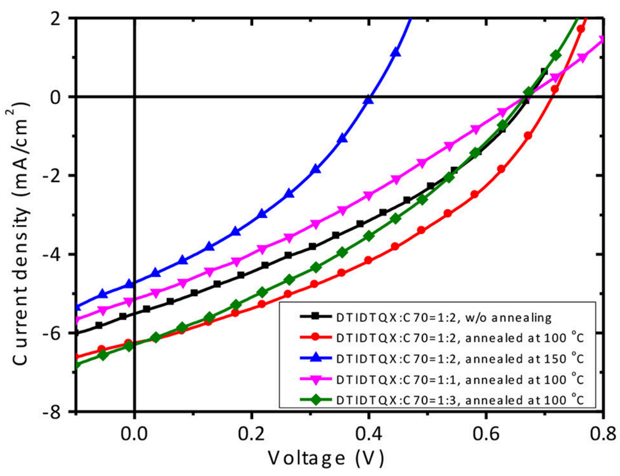

FIGURE 8 | The J-V curves of **DTIDTQX**-based devices.

best **DTRDTQX**-based OSC was realized with the short-circuit current density (J_{sc}) and PCE of 5.66 mA/cm^2 and 1.44%, respectively. The champion **DTRDTQX**-based OSC exhibited almost the same open-circuit voltage (V_{oc}) of ~0.65 V as other OSCs with different weight ratios (1:1 and 1:3) of **DTRDTQX**:C_{70}. Moreover, for the devices based on **DTRDTQX**:C_{70} with the weight ratios of 1:1 and 1:3, the decreased J_{sc} was mainly ascribed to the imbalanced electron and hole diffusion in the OSCs (Kim et al., 2009). The photovoltaic data in **Table 2** implied that the weight ratio (**DTRDTQX**:C_{70}) of 1:2 was advantageous to the photovoltaic performance of **DTRDTQX**:C_{70}-based OSCs. The photovoltaic properties of **DTRDTQX**:C_{70}(1:2)-based OSCs with 150°C thermal annealing and without thermal annealing were also studied and compared. The V_{oc} and PCE of the OSC with 150°C thermal annealing were decreased to 0.51 V and 1.19%, respectively. As to the OSC without thermal annealing, the PCE was decreased to 1.14% and V_{oc} (~0.66V) was almost unchanged compared with the champion **DTRDTQX**-based OSC. Therefore, 100°C thermal annealing treatment was necessary for the reasonable photovoltaic performance of **DTRDTQX**:C_{70}(1:2)-based OSCs according to the experimental data.

As to **DTIDTQX**-based OSCs, the photovoltaic performance was modulated by the weight ratios of **DTIDTQX**:C_{70} from 1:1 to 1:3. When the blend ratio of **DTIDTQX**:C_{70} reached 1:2, the best **DTIDTQX**-based OSC was realized as shown in **Table 2**. The V_{oc}, J_{sc}, FF, and PCE of the champion device were 0.71V, 6.24 mA/cm^2, 0.38 and 1.70%, respectively. It was worthy to note that the V_{oc} of **DTIDTQX**:C_{70}(1:2)-OSC was 0.06 V higher than that of **DTRDTQX**:C_{70}(1:2)-OSC, mainly due to the low-lying HOMO (−5.33 eV) of **DTIDTQX** as shown in **Figure 6**. Moreover, the J_{sc} and PCE of **DTIDTQX**:C_{70}(1:2)-OSC were both higher than those of **DTRDTQX**:C_{70}(1:2)-OSC. Therefore, the photovoltaic properties of **DTIDTQX**-based devices were superior to those of **DTRDTQX**-based counterparts, which was mainly ascribed to the narrow band gap (∼1.37 eV) of **DTIDTQX** and the consequent effective absorption in solar spectrum. The photovoltaic performance of **DTIDTQX**:C_{70}(1:2)-OSC was deteriorated when the active layer was treated with 150°C thermal annealing as shown in **Table 2**. And when **DTIDTQX**:C_{70}(1:2)-OSC was fabricated without thermal annealing, the PCE decreased to 1.26%. Therefore, 100°C thermal annealing was favorable to **DTIDTQX**:C_{70}(1:2)-OSC and a decent PCE of 1.70% was obtained accordingly. However, the FF values of the OSCs were relatively low in this work and much work should be required to further increase FF as well as PCE of the OSCs, such as inserting buffer layers (Ji et al., 2016; Li et al., 2016; Mbuyise et al., 2016), introducing optical spacers (Ben Dkhil et al., 2014), employing solvent annealing (Sun et al., 2014; Li et al., 2015), chemical treatments (Bai et al., 2015), etc.

The morphology of **DTRDTQX**:C_{70}(1:2) and **DTIDTQX**:C_{70}(1:2) films was studied by atomic force microscopy (AFM) (Agilent Series 5500) as shown in **Figure 9**. The root-mean-square roughness (RMS) of **DTIDTQX**:C70

TABLE 2 | Photovoltaic data of the OSCs.

DTRDTQX: C_{70}	Thermal annealing	V_{oc} (V)	J_{sc} (mA/cm^2)	FF	PCE (%)
1:1	100°C	0.66	4.27	0.36	1.01
1:2	100°C	0.65	5.66	0.39	1.44
1:3	100°C	0.64	5.00	0.33	1.05
1:2	150°C	0.51	6.09	0.38	1.19
1:2	w/o	0.66	4.86	0.36	1.14
DTIDTQX: C_{70}					
1:1	100°C	0.67	5.13	0.30	1.02
1:2	100°C	0.71	6.24	0.38	1.70
1:3	100°C	0.67	6.31	0.34	1.43
1:2	150°C	0.40	4.71	0.35	0.66
1:2	w/o	0.67	5.51	0.34	1.26

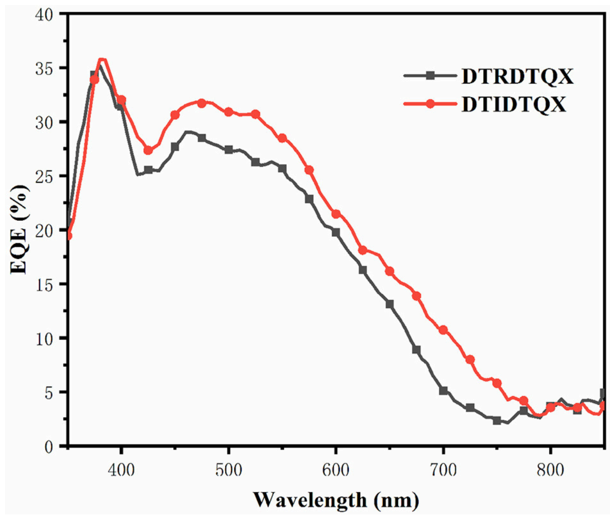

FIGURE 10 | The EQE spectra of **DTRDTQX** and **DTIDTQX**-based devices.

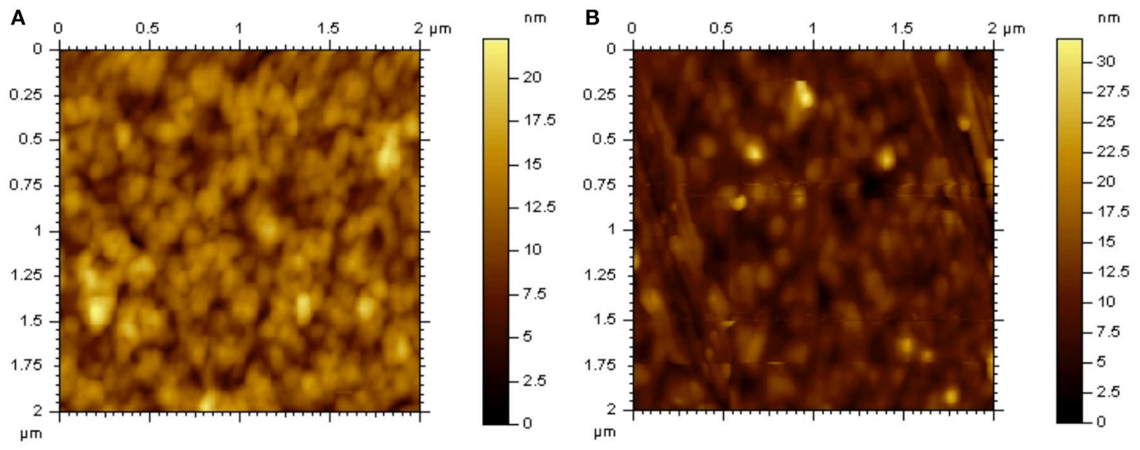

FIGURE 9 | AFM images of **(A) DTRDTQX**:C_{70}(1:2) and **(B) DTIDTQX**:C_{70}(1:2) films.

(1:2) film was 2.94 nm, which was a little higher than that of **DTRDTQX**:C70 (1:2) film (2.58 nm), The relatively low RMS of **DTRDTQX**:C_{70}(1:2) and **DTIDTQX**:C_{70}(1:2) facilitated the reasonable photovoltaic performance of the corresponding devices. Besides, the external quantum efficiency (EQE) spectra of the champion devices were measured with a lock-in amplifier (model SR830 DSP) as shown in **Figure 10**. The EQE of **DTIDTQX**-based device was higher than that of **DTRDTQX**-based counterpart and the integrated photocurrent was 5.47 and 4.71 mA/cm^2, respectively, which was consistent with the photovoltaic properties of the corresponding OSCs. In order to further study the charge transporting properties of the p-type small molecules, hole mobility was measured by using the space-charge-limited current (SCLC) method and the structure of the hole-only devices was ITO/PEDOT:PSS/donor/Au. The $J^{1/2}$-V curves were measured as shown in Supplementary Material. The relation of J and V could be described by $J = 9\varepsilon_0\varepsilon\mu(V_{app}-V_s-V_{bi})^2/8L^3$, where J was the current density, ε_0 was the permittivity of free space, ε was the relative permittivity of the p-type small molecules, μ was the hole mobility, V_{app} was the applied voltage, V_s was the voltage drop from series resistance of the substrate, V_{bi} was the built-in voltage and L was the thickness of the active layers (Qu et al., 2017). The hole mobilities were calculated with the fitted slope of the $J^{1/2}$-V curves, which were $3.62*10^{-6}$ cm^2 V^{-1} s^{-1} and $2.27*10^{-5}$ cm^2 V^{-1} s^{-1} for **DTRDTQX** and **DTIDTQX**, respectively. The hole mobility of **DTIDTQX** was higher than that of **DTRDTQX**, which contributed to the decent photovoltaic performance of **DTIDTQX**-based OSCs. All the experimental data showed that **DTIDTQX** and **DTRDTQX** were promising donor candidates for small molecule OSCs and improved photovoltaic performance of OSCs based on **DTIDTQX** and **DTRDTQX** would be foreseen in the future.

CONCLUSIONS

Two small molecules **DTRDTQX** and **DTIDTQX** with the D-A-A structure were studied in this work. **DTRDTQX** and **DTIDTQX** were used as the donors in bulk-heterojunction solar cells. The optimal OSCs based on **DTRDTQX**:C_{70}(1:2) and **DTIDTQX**:C_{70}(1:2) were achieved with the PCE of 1.44% and 1.70%, respectively. The photovoltaic properties of **DTIDTQX** were superior to those of **DTRDTQX**, which was attributed to the narrow band gap (1.37 eV) and the high hole mobility ($2.27*10^{-5}$ cm^2 V^{-1} s^{-1}) of **DTIDTQX.** Therefore, **DTRDTQX** and **DTIDTQX** would be promising donor materials for organic solar cells in future.

AUTHOR CONTRIBUTIONS

All authors listed have made a substantial, direct and intellectual contribution to the work, and approved it for publication.

FUNDING

This work was supported by the National Natural Science Foundation of China under grant Nos 11574013, U1605244, and 11527901, the National Fund for Fostering Talents of Basic Science (NFFTBS) with grant No. J1030310 and J1103205, the authors also extend their appreciation for the support from the International Scientific Partnership Program ISPP at King Saud University, ISPP#0112.

SUPPLEMENTARY MATERIAL

The Supplementary Material for this article can be found online at: https://www.frontiersin.org/articles/10.3389/fchem.2018.00260/full#supplementary-material

REFERENCES

Bai, S., Jin, Y. Z., Liang, X. Y., Ye, Z. Z., Wu, Z. W., Sun, B. Q., et al. (2015). Ethanedithiol treatment of solution-processed ZnO thin films: controlling the intragap states of electron transporting interlayers for efficient and stable inverted organic photovoltaics. *Adv. Energy Mater.* 5:1401606. doi: 10.1002/aenm.201401606

Ben Dkhil, S., Duche, D., Gaceur, M., Thakur, A. K., Aboura, F. B., Escoubas, L., et al. (2014). Interplay of optical, morphological, and electronic effects of ZnO optical spacers in highly efficient polymer solar cells. *Adv. Energy Mater.* 4:1400805. doi: 10.1002/aenm.201400805

Bijleveld, J. C., Shahid, M., Gilot, J., Wienk, M. M., and Janssen, R. A. J. (2009). Copolymers of cyclopentadithiophene and electron-deficient aromatic units designed for photovoltaic applications. *Adv. Funct. Mater.* 19, 3262–3270. doi: 10.1002/adfm.200900412

Cardona, C. M., Li, W., Kaifer, A. E., Stockdale, D., and Bazan, G. C. (2011). Electrochemical considerations for determining absolute frontier orbital energy levels of conjugated polymers for solar cell applications. *Adv. Mater.* 23, 2367–2371. doi: 10.1002/adma.201004554

Chen, C. C., Chang, W. H., Yoshimura, K., Ohya, K., You, J. B., Gao, J., et al. (2014). An efficient triple-junction polymer solar cell having a power conversion efficiency exceeding 11%. *Adv. Mater.* 26 5670–5677. doi: 10.1002/adma.201402072

Chen, J., and Cao, Y. (2009). Development of novel conjugated donor polymers for high-efficiency bulk-heterojunction photovoltaic devices. *Acc. Chem. Res.* 42, 1709–1718. doi: 10.1021/ar900061z

Chen, J. D., Cui, C., Li, Y. Q., Zhou, L., Ou, Q. D., Li, C., et al. (2015). Single-junction polymer solar cells exceeding 10% power conversion efficiency. *Adv. Mater.* 27, 1035–1041. doi: 10.1002/adma.201404535

Chen, Y. H., Lin, L. Y., Lu, C. W., Lin, F., Huang, Z. Y., Lin, H. W., et al. (2012). Vacuum-deposited small-molecule organic solar cells with high power conversion efficiencies by judicious molecular design and device optimization. *J. Am. Chem. Soc.* 134, 13616–13623. doi: 10.1021/ja301872s

Coughlin, J. E., Henson, Z. B., Welch, G. C., and Bazan, G. C. (2014). Design and synthesis of molecular donors for solution-processed high-efficiency organic solar cells. *Acc. Chem. Res.* 47, 257–270. doi: 10.1021/ar400136b

Gustafsson, G., Cao, Y., Treacy, G. M., Klavetter, F., Colaneri, N., and Heeger, A. J. (1992). Flexible light-emitting-diodes made from soluble conducting polymers. *Nature* 357, 477–479. doi: 10.1038/357477a0

He, Z. C., Xiao, B., Liu, F., Wu, H. B., Yang, Y. L., Xiao, S., et al. (2015). Single-junction polymer solar cells with high efficiency and photovoltage. *Nat. Photonics* 9, 174–179. doi: 10.1038/nphoton.2015.6

Heo, J. H., Song, D. H., Han, H. J., Kim, S. Y., Kim, J. H., Kim, D., et al. (2015). Planar CH3NH3PbI3 perovskite solar cells with constant 17.2% average power conversion efficiency irrespective of the scan rate. *Adv. Mater.* 27, 3424–3430. doi: 10.1002/adma.201500048

Huang, J., Zhang, S., Jiang, B., Chen, Y., Zhang, X., Fan, Z., et al. (2016). Terminal moiety-driven electrical performance of asymmetric small-molecule-based organic solar cells. *J. Mater. Chem. A* 4, 15688–15697. doi: 10.1039/C6TA07450B

Ji, C. H., Jang, J. M., and Oh, S. Y. (2016). Performance of organic photovoltaics using an ytterbium trifluoride n-type buffer layer. *Electr. Mater. Lett.* 12, 301–307. doi: 10.1007/s13391-016-5451-4

Jorgensen, M., and Krebs, F. C. (2005). Stepwise unidirectional synthesis of oligo phenylene vinylenes with a series of monomers. Use in plastic solar cells. *J. Org. Chem.* 70, 6004–6017. doi: 10.1021/jo0506783

Kim, B. J., Miyamoto, Y., Ma, B. W., and Frechet, J. M. J. (2009). Photocrosslinkable polythiophenes for efficient, thermally stable, organic photovoltaics. *Adv. Funct. Mater.* 19, 2273–2281. doi: 10.1002/adfm.200900043

Kim, H. S., Lee, C. R., Im, J. H., Lee, K. B., Moehl, T., Marchioro, A., et al. (2012). Lead iodide perovskite sensitized all-solid-state submicron thin film mesoscopic solar cell with efficiency exceeding 9%. *Sci. Rep.* 2:591. doi: 10.1038/srep00591

Lau, X. B. C., Wang, Z. Q., and Mitra, S. (2013). A C70-carbon nanotube complex for bulk heterojunction photovoltaic cells. *Appl. Phys. Lett.* 103:243108. doi: 10.1063/1.4847376

Li, J. S., Jiu, T. G., Li, B. R., Kuang, C. Y., Chen, Q. S., Ma, S. S., et al. (2016). Inverted polymer solar cells with enhanced fill factor by inserting the potassium stearate interfacial modification layer. *Appl. Phys. Lett.* 108:181602. doi: 10.1063/1.4948585

Li, M., Liu, F., Wan, X., Ni, W., Kan, B., Feng, H., et al. (2015). Subtle balance between length scale of phase separation and domain purification in small-molecule bulk-heterojunction blends under solvent vapor treatment. *Adv. Mater.* 27, 6296–6302. doi: 10.1002/adma.201502645

Lin, L. Y., Chen, Y. H., Huang, Z. Y., Lin, H. W., Chou, S. H., Lin, F., et al. (2011). A low-energy-gap organic dye for high-performance small-molecule organic solar cells. *J. Am. Chem. Soc.* 133, 15822–15825. doi: 10.1021/ja205126t

Liu, Y., Chen, C. C., Hong, Z., Gao, J., Yang, Y. M., Zhou, H., et al. (2013). Solution-processed small-molecule solar cells: breaking the 10% power conversion efficiency. *Sci. Rep.* 3:3356. doi: 10.1038/srep03356

Love, J. A., Proctor, C. M., Liu, J. H., Takacs, C. J., Sharenko, A., van der Poll, T. S., et al. (2013). Film morphology of high efficiency solution-processed small-molecule solar cells. *Adv. Funct. Mater.* 23, 5019–5026. doi: 10.1002/adfm.201300099

Mbuyise, X. G., Tonui, P., and Mola, G. T. (2016). The effect of interfacial layers on charge transport in organic solar cell. *Phys. B Condens. Matter* 496, 34–37. doi: 10.1016/j.physb.2016.05.021

Qu, B., Wu, H., Zhao, B., Liu, H., Gao, C., Qi, X., et al. (2017). An alternating polymer with fluorinated quinoxaline and 2,7-carbazole segments for photovoltaic devices. *RSC Adv.* 7, 16041–16048. doi: 10.1039/C6RA28128A

Roquet, S., Cravino, A., Leriche, P., Aleveque, O., Frere, P., and Roncali, J. (2006). Triphenylamine-thienylenevinylene hybrid systems with internal charge transfer as donor materials for heterojunction solar cells. *J. Am. Chem. Soc.* 128, 3459–3466. doi: 10.1021/ja058178e

Schulze, K., Uhrich, C., Schuppel, R., Leo, K., Pfeiffer, M., Brier, E., et al. (2006). Efficient vacuum-deposited organic solar cells based on a new low-bandgap oligothiophene and fullerene C-60. *Adv. Mater.* 18, 2872–2875. doi: 10.1002/adma.200600658

Shaheen, S. E., Radspinner, R., Peyghambarian, N., and Jabbour, G. E. (2001). Fabrication of bulk heterojunction plastic solar cells by screen printing. *Appl. Phys. Lett.* 79, 2996–2998. doi: 10.1063/1.1413501

Sun, K., Xiao, Z., Hanssen, E., Klein, M. F. G., Dam, H. H., Pfaff, M., et al. (2014). The role of solvent vapor annealing in highly efficient air-processed small molecule solar cells. *J. Mater. Chem. A* 2, 9048–9054. doi: 10.1039/c4ta01125b

Sun, Y., Welch, G. C., Leong, W. L., Takacs, C. J., Bazan, G. C., and Heeger, A. J. (2011). Solution-processed small-molecule solar cells with 6.7% efficiency. *Nat. Mater.* 11, 44–48. doi: 10.1038/nmat3160

Xiao, Y. M., Han, G. Y., Wu, J. H., and Lin, J. Y. (2016). Efficient bifacial perovskite solar cell based on a highly transparent poly(3,4-ethylenedioxythiophene) as the p-type hole-transporting material. *J. Pow. Sour.* 306, 171–177. doi: 10.1016/j.jpowsour.2015.12.003

You, J., Dou, L., Yoshimura, K., Kato, T., Ohya, K., Moriarty, T., et al. (2013). A polymer tandem solar cell with 10.6% power conversion efficiency. *Nat. Commun.* 4:1446. doi: 10.1038/ncomms2411

Zhang, H., Xu, M. F., Cui, R. L., Guo, X. H., Yang, S. Y., Liao, L. S., et al. (2013). Enhanced performance of inverted organic photovoltaic cells using CNTs-TiOX nanocomposites as electron injection layer. *Nanotechnology* 24:355401. doi: 10.1088/0957-4484/24/35/355401

Zhang, S. D., Lei, L., Yang, S. W., Li, X. M., Liu, Y., Gao, Q. Q., et al. (2016). Influence of TiO2 blocking layer morphology on planar heterojunction perovskite solar cells. *Chem. Lett.* 45, 592–594. doi: 10.1246/cl.160059

Zhang, Z. G., Yang, Y., Zhang, S. Y., Min, J., Zhang, J., Zhang, M. J., et al. (2011). Effect of acceptor substituents on photophysical and photovoltaic properties of triphenylamine-carbazole alternating copolymers. *Synth. Met.* 161, 1383–1389. doi: 10.1016/j.synthmet.2011.05.005

Zhou, H., Zhang, Y., Mai, C. K., Collins, S. D., Bazan, G. C., Nguyen, T. Q., et al. (2015). Polymer homo-tandem solar cells with best efficiency of 11.3%. *Adv. Mater.* 27, 1767–1773. doi: 10.1002/adma.201404220

Conflict of Interest Statement: The authors declare that the research was conducted in the absence of any commercial or financial relationships that could be construed as a potential conflict of interest.

The reviewer XZ and handling Editor declared their shared affiliation.